Energy Efficiency Optimization Method of WDM Visible Light Communication System for Indoor Broadcasting Networks

Dayu Shi, *Member, IEEE,* *Xun Zhang, *Senior Member, IEEE,* Ziqi Liu, Xuanbang Chen, Jianghao Li, Xiaodong Liu, *Member, IEEE,,* and William Shieh, *Fellow, IEEE,*

Abstract—This paper introduces a novel approach to optimize energy efficiency in wavelength division multiplexing (WDM) Visible Light Communication (VLC) systems designed for indoor broadcasting networks. A physics-based LED model is integrated into system energy efficiency optimization, enabling quantitative analysis of the critical issue of VLC energy efficiency: the nonlinear interplay between illumination and communication performance. The optimization jointly incorporates constraints on communication quality of each channel, and illumination performance, standardized by the International Commission on Illumination (CIE). The formulated nonlinear optimization problem is solved by the Sequential Quadratic Programming (SQP) algorithm in an experiment-based simulation. An integrated Red-Green-Blue-Yellow Light Emitting Diode (RGBY-LED) is measured for model calibration and three different scenarios are simulated to evaluate the generality of the proposed method. Results demonstrate a double enhancement in performance and a high versatility in accommodating various scenarios. Furthermore, it highlights the importance of balancing communication and illumination imperatives in VLC systems, challenging conventional perceptions focused solely on minimizing power consumption.

Index Terms—Energy Efficiency Optimization, Visible Light Communication, Nonlinearity, LED Modeling.

I. INTRODUCTION

TTH white paper on the sixth generation (6G) architecture landscape from the European perspective is delivered recently [1]. It proposes the main novel trends and principles that will form the backbone of future 6G network architecture and discusses along different axes related to 6G features. One of the most significant architectural enablers is the sustainable network. According to the Sustainable Development Goals (SDG) of the United Nations(UN), the white paper proposes a threefold sustainability from the societal, economic, and environmental targets, which requires reducing more than 30% CO_2 emissions in 6G powered sectors of society, more than 30% total cost of ownership, and more than 90% energy transmitted per bit, respectively.

D. Shi, and W. Shieh are with the School of Engineering, Westlake University, Hangzhou, 310030, China (e-mail: shidayu@westlake.edu.cn, shiehw@westlake.edu.cn).

X. Zhang, Z. Liu, and X. Chen are with the Institut supérieur d'électronique de Paris, Paris 75006, France (e-mail: xun.zhang@isep.fr, ziqi.liu@isep.fr, xuanbang.chen@ext.isep.fr).

X. Liu are with the School of Information Engineering, Nanchang University, Nanchang 330031, China (e-mail: xiaodongliu@ncu.edu.cn).

J. Li is with the School of Physics and Electronics, Shandong Normal University, Jinan 250014, China (e-mail: sdnuljhao@sdnu.edu.cn).

With the strict energy efficiency requirements of the 6G network, revolutionized Internet of Things (IoT) applications require ten or even a hundred times the performance improvement compared to the the fifth generation (5G) era [2]. The expected Key Performance Indicators (KPIs) include the dense of connection 10^7 devices/km^2, the mobile traffic capability $1 \ Gbits/s/m^2$, the network latency 10-100 μs, the energy efficiency $1 \ Tb/J$, etc [3, 4].

Meeting the increasing demands of IoT applications while balancing energy efficiency through conventional wireless communication technologies is a formidable challenge [5]. Visible Light Communication (VLC), modulating visible light to transmit information and simultaneously provide illumination, offers a promising solution [6]. Numerous studies have highlighted the benefits of VLC systems [7, 8, 9]. From a sustainability standpoint, the most compelling feature of VLC systems is energy efficiency, which leverages existing illumination resources for indoor communication services. To maximize this superiority, a complete definition and accurate analysis of VLC energy efficiency are expected for massive-IoT networks in the 6G era.

Existing research on the energy efficiency analysis and optimization of VLC systems are considered from three perspectives. First, some researchers focuses on hybrid systems, encompassing VLC combined with Radio Frequency (RF) [10, 11], Power Line Communication (PLC) [12], and Long Term Evolution (LTE) [13]. Within these contexts, researchers aim to integrate VLC systems with other technologies while maintaining optimal global energy efficiency.

Subsequently, researchers address the energy efficiency of VLC systems within specific scenarios such as Non-Orthogonal Multiple Access (NOMA) [14], heterogeneous networks [15], Multi-Input Multi-Output (MIMO), and broadcasting [16]. These studies elucidate the challenges in enhancing VLC energy efficiency in multi-user environments and offer optimized solutions for resource allocation, including power, subchannels, and spectrum.

Additionally, the other research refines the specific optimization variables, most notably input signal power [24], LED Direct Current (DC) [25], and amplifier gain at the transmitter [26]. These variables are critical for achieving the best energy-efficient configuration of VLC systems. Concurrently, as VLC serves dual functions, illumination and communication, both requirements are integrated as constraints in the optimization process [27]. For a comprehensive understanding of the current

TABLE I: Representative Existing Research of VLC System Energy Efficiency

Paper	Objective System	Objective Scenario	Objective Variable	LED Model	Illumination Requirements
[17]	Hybrid VLC/RF	MIMO	Signal Power	Constant	None
[12]	Hybrid VLC/RF/PLC	Broadcasting	Signal Power	Constant	None
[18]	Multi-LED VLC	Broadcasting	Signal Power	Constant	Illumination Intensity
[19]	VLC	MIMO	Signal Power	Constant	Illumination Intensity
[20]	VLC	MIMO	Amplifier Gain	Linear	Illumination Intensity
[21]	VLC	MIMO	Signal Power	Low-Pass	None
[22]	VLC	Broadcasting	LED's Current	Empirical Formula	Illumination Intensity
[23]	VLC/SLIPT	MIMO	LED's Current/Signal Power	Linaer	Illumination Intensity

research of VLC system energy efficiency, the representative existing research is detailed in Tab. I.

The related works exhibit excellent performance in optimizing VLC system performance, whereas there still remain several research gaps toward applying to practical VLC system energy efficiency optimization.

First, existing research predominantly treats VLC systems as electronic systems, thereby focusing on optimizing the signal power to achieve optimal energy efficiency. Whereas VLC systems work as electro-optical systems, providing both illumination and communication services simultaneously. Its energy efficiency optimization must concurrently evaluate the illumination and communication power consumption to solve the optimal configuration of the system, reaching the global maximum energy efficiency.

Second, empirical measurements confirm a nonlinear interplay between illumination and communication performance in VLC systems, attributable to the LED's intrinsic nonlinearity [28, 29]. Current research overlooks this interplay due to their LED models established by a constant parameter or any mathematical formula without physical significance. Few researchers employ a physics-based LED in their system model to quantify this interplay in their optimization, resulting in suboptimal optimization results.

Third, the majority of existing methods have not adequately incorporated indoor illumination requirements, such as illuminance and color, into their optimization algorithms. These values are regulated by the International Commission on Illumination (CIE) standards to ensure human ocular safety across various scenarios [30]. Thus, the indoor illumination indicators should be formulated into functions and applied to the optimization as constraints.

Last, the polychromatic LED-based wavelength division multiplexing (WDM) VLC systems perform extremely high data rates and illumination efficiency [31]. Especially the Red-Green-Blue-Yellow (RGBY)-LED-based WDM VLC transmission reached the data rate of 15.73 $Gbit/s$ [32], becoming the most potential architecture in future VLC system applications. Additional merits include improved signal quality, facilitated by optimizing multiple color channels for varying transmission conditions, and increased fault tolerance through redundant data pathways [33]. However, the existing optimization method fails to be implemented for WDM VLC systems due to the lack of an appropriate system model.

This paper proposed a novel optimization method for the RGBY-LED-based WDM VLC broadcasting system. Addressing the limitations identified in existing research, the contributions of the proposed optimization method are summarized as follows.

- A physics-based LED model, developed in our previous work [34], is employed to accurately characterize the nonlinear interplay between illumination and communication performance of VLC systems. The LED model integrated with the channel and receiver model forms a WDM VLC system model, serving as the fundamental function of energy efficiency optimization.

- Based on the system model, the proposed optimization method jointly evaluates the power consumption of illumination and communication services. The illuminance of each LED, the Bit Error Rate (BER) of each color channel, and the visual color of the mixed light are formulated as constraint functions applied to the optimization problem, forcing the results satisfying both indoor illumination standards and communication quality requirements across diverse scenarios.

- The formulated nonlinear optimization problem is solved by the Sequential Quadratic Programming (SQP) algorithm in an experiment-based simulation. An integrated RGBY-LED is measured in a VLC transmission testbed to calibrate the LED model applied to the optimization. An indoor VLC broadcasting scenario with different use-cases are simulated to evaluate the performance and generality of the proposed method.

II. WDM VLC SYSTEM MODEL

Fig. 1 delineates the architecture of the RGBY-LED-based WDM VLC broadcasting system. This system incorporates four sub-LEDs—red, green, blue, and yellow—into a single RGBY-LED unit. Data are concurrently transmitted across these four color channels, forming a WDM mechanism. Additionally, the sub-LEDs individually generate calibrated ratios of red, green, blue, and yellow light, which combine to create white light suitable for indoor illumination.

In the transmission process, the bitstream is partitioned into four separate flows. Each flow is mapped onto M-order Quadrature Amplitude Modulation (QAM) and Orthogonal Frequency Division Multiplexing (OFDM) symbols to create
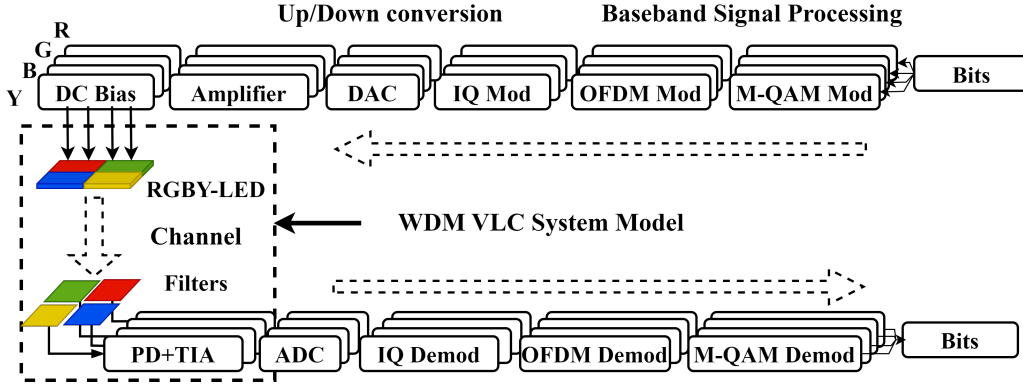
Fig. 1: Schematic diagram of the RGBY-LED-based WDM VLC broadcasting system.

the baseband signals. Utilizing In-phase and Quadrature (IQ) modulation and applying a Digital Analog Converter (DAC) to each channel, these baseband signals are upconverted to higher frequencies and transformed into analog signals. Within each channel, the signal is amplified and added with DC components before transmitting by the corresponding sub-LED. Over the optical wireless channel, the signal of each color is filtered and then detected by the Photodiode (PD), which converts the optical signals back into current signals. A Trans-Impedance Amplifier (TIA) is used to amplify these current signals and convert them into voltage signals. After undergoing down-conversion and demodulation, the original bits are reconstructed.

In this paper, the established WDM VLC system model consists of the RGBY-LED model, channel model, and receiver model, covering the main configurable components of VLC systems. Without loss of generality, the rest are temporarily considered constantly and ideally. The detailed derivation of the system model is separately introduced as follows.
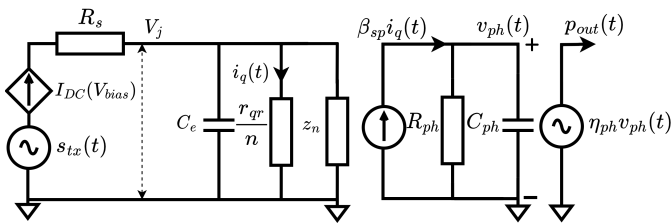

Fig. 2: Simplified small signal equivalent circuit of LEDs.

A. GaN MQW LED Model

A monochromatic LED model is developed and demonstratively verified in our previous work [34]. Based on the theory, the model of RGBY-LED is topologized in this section. Considering each quantum well has the same structure and size, the small signal equivalent circuit of the LED is simplified as Fig. 2. For illustrative convenience, assuming a monochromatic LED featured n quantum wells structure, at bias voltage V_{bias}, its output illuminance (Φ_{LED}) and signal response (h_{led}) are represented by:

$$\Phi_{LED}(V_{bias}) = \frac{638}{A_{rec}} \int_{380}^{830} \mathcal{V}(\lambda) P_L(V_{bias}, \lambda) d\lambda \quad (1)$$

$$h_{led}(V_{bias}, t) = \mathcal{L}^{-1}(H(V_{bias}, \boldsymbol{s})) \cdot \exp\left(\frac{-4(\lambda - \lambda_0)^2}{(\Delta\lambda)^2}\right)$$
$$= \frac{a_1(V_j)}{a_4(V_j) - a_2 \cdot a_3(V_j)} \cdot \left[\exp\left(\frac{-a_3(V_j) \cdot t}{a_4(V_j)}\right) - \exp\left(\frac{-t}{a_2}\right)\right]$$
$$\cdot \exp\left(\frac{-4(\lambda - \lambda_0)^2}{(\Delta\lambda)^2}\right)$$
$$(2)$$

$$P_L(V_{bias}, \lambda) = a_5(V_j) \cdot \exp\left(\frac{-4(\lambda - \lambda_0)^2}{(\Delta\lambda)^2}\right) \quad (3)$$

$$H_{led}(V_{bias}, \boldsymbol{s}) = \frac{p_{out}(\boldsymbol{s})}{s_{tx}(\boldsymbol{s})} = \frac{a_1}{(1 + a_2 \cdot \boldsymbol{s})(a_3 + a_4 \cdot \boldsymbol{s})} \quad (4)$$

$$V_j = V_{bias} - R_s I_{DC} \quad (5)$$

$$I_{DC} = I_s(\exp(\frac{q(V_{bias} - R_s I_{DC})}{\eta k_B T}) - 1) \quad (6)$$

where, P_L represents the LED's optical spectrum, calculated as Eq. (3), and $\mathcal{V}$ is the luminosity function defined by the CIE [35]. The power transfer function of the LED is denoted as H_{led}, derived as Eq. (4), and the inverse Laplace Transform operator is $\mathcal{L}^{-1}$. Parameters λ, λ_0, and $\Delta\lambda$ refer to the wavelength range, peak wavelength, and spectrum bandwidth of the emitted light. The power distribution of the LED's emitted light is modeled using a Gaussian distribution [36]. To clearly illustrate, the equations describe the LED's internal physics are replaced by the parameter functions a_1 to a_5, and their expansion are detailed in the Appendix.

For an RGBY-LED, the output illuminance ($\Phi_{LED}^{R,G,B,Y}$), in units of Lux (lx), and the four-channel signal response ($h_{led}^{R,G,B,Y}$) are calculated by:

$$\Phi_{LED}^{R,G,B,Y} = \frac{638}{A_{rec}} \int_{380}^{830} \mathcal{V}(\lambda) P_L^{R,G,B,Y} (V_{bias}^{R,G,B,Y}) d\lambda \quad (7)$$

$$h_{led}^{R,G,B,Y}(V_{bias}^{R,G,B,Y},t) = \begin{pmatrix} h_{led}^R(V_{bias}^R,t) \\ h_{led}^G(V_{bias}^G,t) \\ h_{led}^B(V_{bias}^B,t) \\ h_{led}^Y(V_{bias}^Y,t) \end{pmatrix} \quad (8)$$

To further characterize the illumination performance of the RGBY-LED, the visual color of the mixed light is evaluated by the Correlated Color Temperature (CCT). An empirical function [37] is used to calculate its value as:

$$CCT = 437 \cdot \hat{n}^3 + 3601 \cdot \hat{n}^2 + 6861 \cdot \hat{n} + 5517 \quad (9)$$

$$\hat{n} = \frac{\hat{x} - 0.3320}{0.1858 - \hat{y}} \quad (10)$$

$$\hat{x} = \frac{\int_{380}^{830} \bar{x}(\lambda) P_L^{R,G,B,Y}(\lambda)d\lambda}{\int_{380}^{830} P_L^{R,G,B,Y}(\lambda)(\bar{x}(\lambda) + \bar{y}(\lambda) + \bar{z}(\lambda))d\lambda} \quad (11)$$

$$\hat{y} = \frac{\int_{380}^{830} \bar{y}(\lambda) P_L^{R,G,B,Y}(\lambda)d\lambda}{\int_{380}^{830} P_L^{R,G,B,Y}(\lambda)(\bar{x}(\lambda) + \bar{y}(\lambda) + \bar{z}(\lambda))d\lambda} \quad (12)$$

$$V_{bias}^{R,G,B,Y} = (V_{bias}^R, V_{bias}^G, V_{bias}^B, V_{bias}^Y) \quad (13)$$

$$P_L^{R,G,B,Y}(V_{bias}^{R,G,B,Y}) = P_L^R(V_{bias}^R,\lambda) + P_L^G(V_{bias}^G,\lambda) \\ + P_L^B(V_{bias}^B,\lambda) + P_L^Y(V_{bias}^Y,\lambda) \quad (14)$$

Where, $V_{bias}^{R,G,B,Y}$ represents the bias voltage applied to each color LED as shown in Eq. (13). $P_L^{R,G,B,Y}(V_{bias}^{R,G,B,Y})$ denotes the total output power of the RGBY-LED, in units of Watt. $x(\lambda)$, $y(\lambda)$, $z(\lambda)$ are the color matching functions provided by CIE [35].
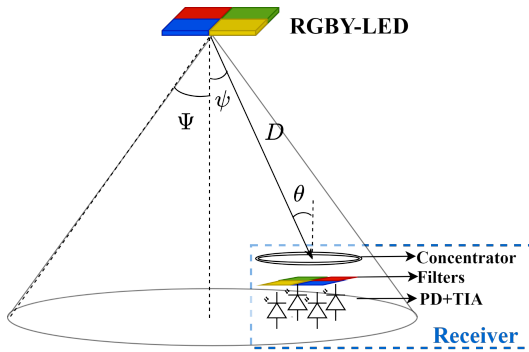

Fig. 3: Schematics of the channel and receiver.

B. Channel and Receiver Model

The schematic diagram of the channel and receiver in the WDM VLC system is presented in Fig. 3. In the channel model, the optical signal is assumed to propagate in a LOS manner, and a Lambertian radiation model [38] characterizes the path loss during light propagation, given by:

$$h_c = \begin{cases} \delta(t) \cdot \frac{(\mu+1)A_{rec} \cdot cos(\psi)^\mu cos(\theta)}{2\pi D^2} & 0 \le \psi \le \psi_{FOV} \\ 0 & \text{otherwise} \end{cases} \quad (15)$$

$$\mu = \frac{\ln 2}{\ln(\cos \Psi)} \quad (16)$$

Parameters ψ and θ represent the transmit and receive angles, while D, μ, and A_{rec} refer to the distance between the transmitter and receiver, Lambertian radiant order, and the effective receiver area, respectively. Symbols Ψ and ψ_{FOV} denote the half-power angle of the LED and the FOV (Field of View) of the receiver.

The receiver setup includes an optical concentrator, an optical filter, and four PDs integrated with TIAs for each channel. In the receiver model, the received signal is computed by integrating the photo-sensitivity of the PDs ($\kappa(\lambda)$) with the filtered optical signal, then multiplying by the gain of the TIA (G_{TIA}) and optical concentrator (G_{opt}). The optical filters for each channel are represented as H_{filter}, and an ideal rectangular filter is used in the model. Parameters Γ_p, $\hat{\lambda}_c$, and $\Delta\hat{\lambda}$ denote the filter loss, peak wavelength, and bandwidth, respectively.

$$h_{rx}^{R,G,B,Y}(\lambda) = \begin{pmatrix} h_{rx}^R(\lambda) \\ h_{rx}^G(\lambda) \\ h_{rx}^B(\lambda) \\ h_{rx}^Y(\lambda) \end{pmatrix} \quad (17)$$

$$h_{pd}(\lambda) = G_{TIA}G_{opt} \cdot \int \kappa(\lambda) \cdot H_{filter}(\lambda)d\lambda \quad (18)$$

$$H_{filter}(\lambda) = \Gamma_p\text{rect}(\frac{\lambda - \hat{\lambda}_c}{\Delta\hat{\lambda}}) \quad (19)$$

$$\text{rect}(\lambda) = \begin{cases} 1 & |\lambda| \le \frac{1}{2} \\ 0 & |\lambda| > \frac{1}{2} \end{cases} \quad (20)$$

Combining the above RGBY-LED model, channel model, and receiver model, the illuminance at the receiver side (Φ_{Rx}^{TL}) and the response of WDM VLC system ($h_{vlc}^{R,G,B,Y}$) are represented by Eq. (21) and (22), respectively. While the operators $\times$ and $\otimes$ denote the matrix multiplication and convolution.

$$\Phi_{Rx}^{TL} = \int_{-\infty}^{\infty} \Phi_{Rx}^{R,G,B,Y} \cdot h_c(t,D,\psi,\theta)dt \quad (21)$$

$$h_{vlc}^{R,G,B,Y} = \begin{pmatrix} h_{vlc}^R(V_{bias}^R,t,\psi,\theta,D,\lambda) \\ h_{vlc}^G(V_{bias}^G,t,\psi,\theta,D,\lambda) \\ h_{vlc}^B(V_{bias}^B,t,\psi,\theta,D,\lambda) \\ h_{vlc}^Y(V_{bias}^Y,t,\psi,\theta,D,\lambda) \end{pmatrix}$$

$$= \begin{pmatrix} h_{rx}^R & h_{rx}^R & h_{rx}^R & h_{rx}^R \\ h_{rx}^G & h_{rx}^G & h_{rx}^G & h_{rx}^G \\ h_{rx}^B & h_{rx}^B & h_{rx}^B & h_{rx}^B \\ h_{rx}^Y & h_{rx}^Y & h_{rx}^Y & h_{rx}^Y \end{pmatrix} \times \begin{pmatrix} h_{led}^R \otimes h_c \\ h_{led}^G \otimes h_c \\ h_{led}^B \otimes h_c \\ h_{led}^Y \otimes h_c \end{pmatrix} \quad (22)$$

III. WDM VLC System Energy Efficiency

As a combined illumination and communication system, the WDM VLC system exhibits unique properties that differentiate its energy efficiency calculation from conventional wireless communication systems. In this context, the denominator of the efficiency expression should encompass not only the power expended during data transmission but also factor in the illumination power. Furthermore, the WDM system accommodates multiple channels that concurrently transmit data. Given the distinct characteristics of each color LED, individual channel configurations are adjusted to optimize performance [31]. As a result, the channel capacity of each color is computed individually and subsequently aggregated to yield the overall system throughput. Each channel is simultaneously optimized to ensure global performance, adhering to constraints imposed by both communication Quality of Service (QoS) and indoor illumination requirements.

A. Energy Efficiency Definition

The energy efficiency of the WDM VLC system (EE^{TL}) is defined as the total channel capacity (C^{TL}) of the R, G, B, and Y channels divided by the total power consumption for illumination ($P_{ill}^{R,G,B,Y}$) and communication ($P_{com}^{R,G,B,Y}$), given by:

$$
\begin{aligned}
EE^{TL} &= \frac{C^{TL}}{P_{com}^{R,G,B,Y} + P_{ill}^{R,G,B,Y}} \\
&= \frac{C^R + C^G + C^B + C^Y}{P_{com}^{R,G,B,Y} + P_{ill}^{R,G,B,Y}}
\end{aligned}
\tag{23}
$$

$$
\begin{aligned}
C^{TL} = {} & B^R \cdot \log_2(1 + \frac{(s_{rx}^R(t))^2}{\sigma_{th}^2 + \sigma_{shot}^2}) \\
& + B^G \cdot \log_2(1 + \frac{(s_{rx}^G(t))^2}{\sigma_{th}^2 + \sigma_{shot}^2}) \\
& + B^B \cdot \log_2(1 + \frac{(s_{rx}^B(t))^2}{\sigma_{th}^2 + \sigma_{shot}^2}) \\
& + B^Y \cdot \log_2(1 + \frac{(s_{rx}^Y(t))^2}{\sigma_{th}^2 + \sigma_{shot}^2})
\end{aligned}
\tag{24}
$$

Considering the thermal noise (σ_{th}) and shot noise (σ_{shot}) at the receiver [39], the channel capacity C is expressed by Shannon's law [40] using the Signal Noise Ratio (SNR) in Eq. (24).

$$
s_{rx}^{R,G,B,Y} = \begin{pmatrix} s_{rx}^R \\ s_{rx}^G \\ s_{rx}^B \\ s_{rx}^Y \end{pmatrix} = \begin{pmatrix} h_{vlc}^R \otimes s_{tx}^R \cdot G_{amp}^R \\ h_{vlc}^G \otimes s_{tx}^G \cdot G_{amp}^G \\ h_{vlc}^B \otimes s_{tx}^B \cdot G_{amp}^B \\ h_{vlc}^Y \otimes s_{tx}^Y \cdot G_{amp}^Y \end{pmatrix}
\tag{25}
$$

$$
\begin{aligned}
P_{ill}^{R,G,B,Y} = {} & V_{bias}^R \cdot I_{DC}^G + V_{bias}^G \cdot I_{DC}^G \\
& + V_{bias}^B \cdot I_{DC}^R + V_{bias}^Y \cdot I_{DC}^Y
\end{aligned}
\tag{26}
$$

$$
\begin{aligned}
P_{com}^{R,G,B,Y} = {} & (s_{tx}^R G_{amp}^R)^2 + (s_{tx}^G G_{amp}^G)^2 \\
& + (s_{tx}^B G_{amp}^B)^2 + (s_{tx}^Y G_{amp}^Y)^2
\end{aligned}
\tag{27}
$$

Assuming the generated signals after DAC processing are represented by s_{tx}. The following amplifiers increase its power

in G_{amp} times. The received signal $s_{rx}^{R,G,B,Y}$ is formulated by Eq. (25) and the power consumption of the illumination and communication of four LEDs are calculated as Eq. (26) and (27).

B. Energy Efficiency Optimization

In the context of the energy efficiency definition for the WDM VLC system, the bias voltages ($V_{bias}^{R,G,B,Y}$) directly influence signal response and illumination intensity. Meanwhile, the amplifier gains ($G_{amp}^{R,G,B,Y}$) controls the initial signal power of the VLC system, significantly impacting the magnitude of the SNR. As these parameters operating at the system's transmitter, they can be dynamically reconfigured based on the user's requirements. Therefore, they are selected as optimization variables, given by:

$$
V_{bias}^{R,G,B,Y} = [V_{bias}^R, V_{bias}^G, V_{bias}^B, V_{bias}^Y]
\tag{28}
$$

$$
G_{amp}^{R,G,B,Y} = [G_{amp}^R, G_{amp}^G, G_{amp}^B, G_{amp}^Y]
\tag{29}
$$

$$
\begin{aligned}
& \mathbb{EE}^{\mathbb{TL}}(V_{bias}^{R,G,B,Y}, G_{amp}^{R,G,B,Y}) = \\
& \frac{C^{R,G,B,Y}(V_{bias}^{R,G,B,Y}, G_{amp}^{R,G,B,Y})}{P_{ill}^{R,G,B,Y}(V_{bias}^{R,G,B,Y}) + P_{com}^{R,G,B,Y}(G_{amp}^{R,G,B,Y})}
\end{aligned}
\tag{30}
$$

The objective function of the energy efficiency optimization is represented by Eq. (30). In order to guarantee both the QoS of data transmission and compliance with indoor illumination standards during optimization, several constraints are outlined as follows:

- Adequate Illuminance: The illuminance at the user's location (Φ_{Rx}^{TL}) must exceed the user-required illuminance (Φ_{Rx}^{req}).

- Controlled Light Color: Excessive levels of blue light can be detrimental to human eyes [41]. The CCT of the RGBY-LED should remain below the upper limit set by indoor illumination standards [35].

- Assured Data Transmission QoS: The BER of each channel should remain below the thresholds specified by the communication protocol requirements.

C. Problem Formulation

Based on the previously stated definitions, the objective function, and the constraints involved in energy efficiency optimization for the WDM VLC system, the optimization problem incorporating these constraints can be formulated as:

$$\begin{aligned}
\max \quad & \mathbb{EE}^{\mathbb{TL}}(\boldsymbol{V}_{bias}^{R,G,B,Y}, \boldsymbol{G}_{amp}^{R,G,B,Y}) \\
s.t. \quad & \Phi_{Rx}(\boldsymbol{V}_{bias}^{R,G,B,Y}) \geq \Phi_{Rx}^{req} \\
& BER^R(\boldsymbol{V}_{bias}^{R}, \boldsymbol{G}_{amp}^{R}) \leq BER^{req} \\
& BER^G(\boldsymbol{V}_{bias}^{G}, \boldsymbol{G}_{amp}^{G}) \leq BER^{req} \\
& BER^B(\boldsymbol{V}_{bias}^{B}, \boldsymbol{G}_{amp}^{B}) \leq BER^{req} \\
& BER^Y(\boldsymbol{V}_{bias}^{Y}, \boldsymbol{G}_{amp}^{Y}) \leq BER^{req} \\
& CCT(\boldsymbol{V}_{bias}^{R,G,B,Y}) \leq CCT^{req} \\
& \boldsymbol{V}_{bias}^{R,G,B,Y} \in \{V_{th}^{R,G,B,Y}, V_{max}^{R,G,B,Y}\} \\
& \boldsymbol{G}_{amp}^{R,G,B,Y} \in \{G_{th}^{R,G,B,Y}, G_{max}^{R,G,B,Y}\}
\end{aligned}$$

$$(31)$$

where, the total illuminance at the user's position (Φ_{Rx}^{TL}) is given by:

$$\begin{aligned}
\Phi_{Rx}^{TL}(\boldsymbol{V}_{bias}^{R,G,B,Y}) =& \Phi_{Rx}^{R}(\boldsymbol{V}_{bias}^{R}) + \Phi_{Rx}^{G}(\boldsymbol{V}_{bias}^{G}) \\
& + \Phi_{Rx}^{B}(\boldsymbol{V}_{bias}^{B}) + \Phi_{Rx}^{Y}(\boldsymbol{V}_{bias}^{Y})
\end{aligned} \quad (32)$$

$$BER(\boldsymbol{V}_{bias}, \boldsymbol{G}_{amp}) = \frac{4}{\log_2(M)}(1 - \frac{1}{\sqrt{M}})$$
$$\cdot Q\left(\sqrt{\frac{3\log_2(M)}{M-1}}\mathrm{SNR}(\boldsymbol{V}_{bias}, \boldsymbol{G}_{amp})\right) \quad (33)$$

$$Q(x) = \frac{1}{2}\mathrm{erfc}\left(\frac{x}{\sqrt{2}}\right) \quad (34)$$

Here, considering the WDM VLC system using different orders of QAM signal, the BER is evaluated by the order M with the Q-function [42]. The Q-function represents the tail distribution of the standard normal distribution [43], as shown in Eq. (34). The expansion of all the constraint equations are derived in the Appendix.

For convenient solving the optimization problem, define the functions $f = -\mathbb{EE}^{\mathbb{TL}}$, $g_1 = \Phi_{Rx}^{req} - \Phi_{Rx}^{TL}$, g_2 through g_5 linked to $BER^{R,G,B,Y} - BER^{req}$, and $g_6 = CCT - CCT^{req}$. The optimization variable and the corresponding boundary set are defined as X and X_{set}. The previous expression (Eq. (31)) is reformulated into a standard form given by:

$$\begin{aligned}
\min_{\boldsymbol{X} \in \boldsymbol{X}_{set}} \quad & f(\boldsymbol{X}) \\
s.t. \quad & g_i(\boldsymbol{X}) \leq 0, i = 1, 2, ..., 6
\end{aligned} \quad (35)$$

$$G = [\nabla g_1(\boldsymbol{X}_k), \nabla g_2(\boldsymbol{X}_k), ..., \nabla g_6(\boldsymbol{X}_k)]^T \quad (36)$$

$$h = [-g_1(\boldsymbol{X}_k), -g_2(\boldsymbol{X}_k), ..., -g_6(\boldsymbol{X}_k)]^T \quad (37)$$

The above nonlinear optimization problem with nonlinear constraints in Eq. (35) is tentatively solved by the Sequential Quadratic Programming (SQP) algorithm [44] to validate our proposed optimization method. The advanced algorithms will be discussed and implemented in our future work. The processing step is structured in Algorithm. 1.

where matrix $\boldsymbol{c}$ is defined as $\boldsymbol{c} = \nabla f(\boldsymbol{X}_k)$. $\boldsymbol{p}^{(k)}$ is the optimal step defined as $\boldsymbol{p}^{(k)} = \boldsymbol{X} - \boldsymbol{X}_k$. $\boldsymbol{\mu}$ is the matrix of the Lagrange Multipliers for the six constraints (g_1 to g_6).

Algorithm 1 Sequential Quadratic Programming (SQP)

1: **Initialization:** Choose an initial feasible point $\boldsymbol{X}^{(0)}$, the tolerance ϵ. Set $k = 0$. Calculate $\boldsymbol{H}^{(0)}$.
2: **while** not converged **do**
3:     **Linearize Constraints and Objective:** Approximate $g(\boldsymbol{X})_i$ and $f(\boldsymbol{X})$ by Taylor expansion around $\boldsymbol{X}^{(k)}$.
4:     **Solve Quadratic Subproblem:**

$$\text{minimize}_{\boldsymbol{p}^{(k)}} \quad \frac{1}{2}(\boldsymbol{p}^{(k)})^T\boldsymbol{H}\boldsymbol{p}^{(k)} + \boldsymbol{c}^T\boldsymbol{p}^{(k)}$$
$$\text{subject to} \quad \boldsymbol{G}\boldsymbol{p}^{(k)} \leq \boldsymbol{h}$$

5:     **Results:** $\boldsymbol{p}^{(k)}$ and $\boldsymbol{\mu}^{(k)}$
6:     **Line Search:** Determine $\alpha^{(k)}$ via line search.
7:     **Update:** Set $\boldsymbol{X}^{(k+1)} = \boldsymbol{X}^{(k)} + \alpha^{(k)}\boldsymbol{p}^{(k)}$.
8:     **Hessian Update:** Update $\boldsymbol{H}^{(k+1)}$.
9:     **Check Convergence:** If $\|\nabla f(\boldsymbol{X}^{(k+1)})\| < \epsilon$, terminate.
10: **end while**

$\boldsymbol{H}$ is an approximation to the Hessian matrix of the Lagrangian. The Broyden-Fletcher-Goldfarb-Shanno (BFGS) method [45] is used to update the Hessian approximation $\boldsymbol{H}_{k+1}$. Here, $\boldsymbol{s}_k = \boldsymbol{x}_{k+1} - \boldsymbol{x}_k$ and $\boldsymbol{y}_k = \nabla f(\boldsymbol{x}_{k+1}) - \nabla f(\boldsymbol{x}_k)$. Upon solving each Quadratic Programming (QP) subproblem by the KKT conditions, $\boldsymbol{p}^{(k)}$ is obtained, which is then used to update the current solution to the next iteration as $\boldsymbol{X}_{k+1} = \boldsymbol{X}_k + \alpha_k\boldsymbol{p}^{(k)}$. Where α_k is a step size determined via a line search.

IV. VALIDATION

This section illustrates the validation process in which the proposed energy efficiency optimization method is evaluated based on an experimental-based simulation. Initially, the electroluminescent characteristics and signal power loss of the RGBY-LED model are calibrated by experimental measurements. Subsequently, an indoor broadcasting scenario with different use-cases are simulated to assess the performance and generality of the proposed optimization method.

A. RGBY-LED Model Calibration

A integrated RGBY-LED [46] serves as the sample LED which consists of four monochromatic sub-LEDs, each with its dedicated control pin. Employing it into a VLC transmission link testbed, the electroluminescent properties of each individual sub-LEDs and the signal power loss across each color channel are measured and fitted with the theoretical derivation.

1) RGBY-LED Electroluminescence: Each sub-LED is measured separately with the applied bias voltages and output irradiance ($W \cdot m^{-2}$) by an accurate power source in conjunction with a photometer. The measured data are fitted with the theoretical LED model, shown in Fig. 4.

In the figure, the subscript m and est denote the measured and fitted electroluminescence. The fitting results are consistent with the measurement and show the significantly different electroluminescence between each sub-LED. It emphasizes that the unique physical properties of each LED should neither
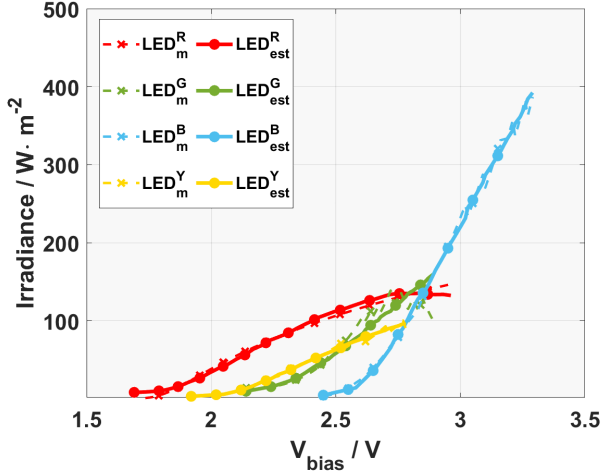
Fig. 4: Electroluminescent characteristics of the RGBY-LED.

Fig. 6: Signal power loss of four-color channels.

be simplified nor overlooked. A physics-based LED model is significant for any upper-layer analysis of VLC system.
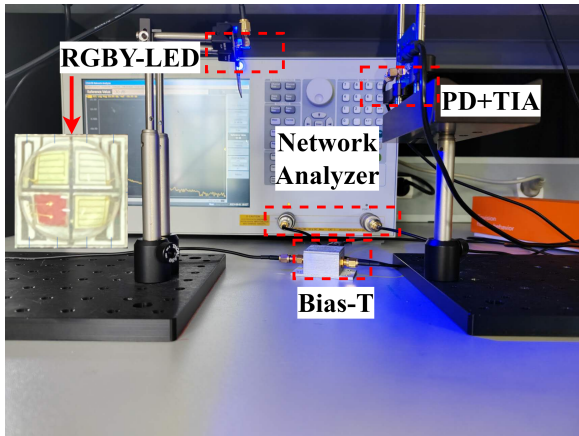

Fig. 5: VLC transmission link testbed.

2) Signal Power Loss over Channels: In the VLC transmission testbed, illustrated in Fig. 5, each color channel is separately evaluated for signal power loss using a Network Analyzer. The analyzer generates a frequency-swept signal ranging from 300 KHz to 50 MHz, which is then added on varying bias voltages by a Bias-T. This signal is transmitted over the LED, through the optical wireless channel, and finally received by an optical receiver, consisting of a PD and TIA, to calculate the signal power loss. The distance between the LED and the receiver is fixed on 10 cm.

Fig. 6 illustrates the measured and model estimated signal power loss, under varying signal frequency and applied bias voltage, across the four-color channels. The comparison reveals that the proposed WDM VLC system model accurately characterizes the signal transmission properties for each color channel. Minor discrepancies between the measured and estimated signal power losses are attributed to the tolerances of the measuring equipment.
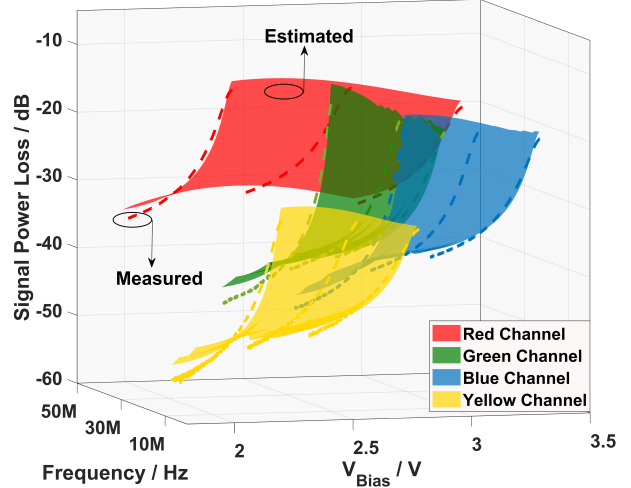
The surface trends in the figure validate two key inferences of the proposed system model: (a) Each channel demonstrates a nonlinear frequency attenuation which arises from the unique physical properties of each monochromatic LED. (b) Signal power loss escalates with increasing bias voltage, owing to the interplay of the LED between providing different illumination intensity and transmitting signals. The proposed RGBY-LED model accurately characterizes this interplay of each channel, supporting accurate and practical energy efficiency optimization.

B. Energy Efficiency Optimization Simulation

The calibrated RGBY-LED model is programmed into the simulation in which an indoor WDM VLC broadcasting system is established, shown in Fig. 7. In the simulation, the parameters calibrated from measurements are marked with symbol *, listed in the Tab. II, and the rest are generated following typical values [47].
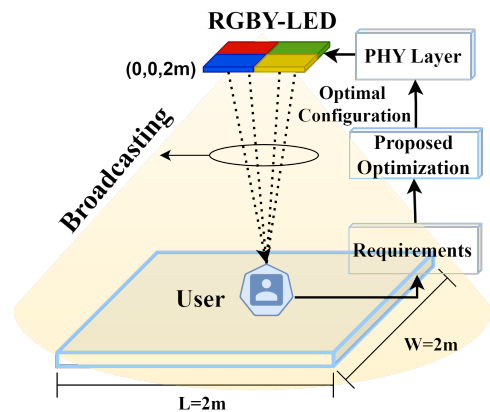

Fig. 7: Schematic of the indoor WDM VLC broadcasting system.

TABLE II: Parameters of the simulation setup

Parameters (*: Calibrated from measurements)	Values
Simulation area	$2m \times 2m \times 2m$
*Bias voltage of the LED ($V_{bias}^{R,G,B,Y}$)	$V_{bias}^{R} \in [1.99, 2.96]V$ $V_{bias}^{G} \in [2.41, 2.89]V$ $V_{bias}^{B} \in [2.72, 3.29]V$ $V_{bias}^{Y} \in [2.20, 2.78]V$
*Central wavelength of the LED's output light ($\lambda_0^{R,G,B,Y}$)	(629,525,460,556) nm
*Optical spectrum bandwidth of the LED ($\Delta\lambda^{R,G,B,Y}$)	(60,65,70,80) nm
Modulation orders of QAM (M)	16/32/64
Bandwidth of OFDM signals	3.84 MHz
Number of subcarriers and OFDM symbols	256×100
Initial signal average power (P_0)	2 dBm
The noise floor of the system (P_{noise})	-120 dBm
Range of amplification gain ($G_{amp}^{R,G,B,Y}$)	[0,20] dB
Central wavelength of the optical filter ($\hat{\lambda}_c$)	(629,525,460,556) nm
Bandwidth of the optical filter	ideal
Coefficient of the optical filter loss (Γ_p)	0.8
Gain of the optical concentrator (G_{opt})	20 dB
Lambert radiation coefficient (m)	1.5
*Effective area of the receiver (A_{rec})	$7.6 \times 10^{-6} m^2$
*FOV of the LED	$60°$

1) Simulation Setup: The simulation background is defined as a user receiving the broadcasting OFDM signals from an RGBY-LED-served WDM VLC system. The broadcasting coverage is a $2m \times 2m$ area, and the RGBY-LED is suspended from a $2m$ height ceiling. The proposed optimization method solves the optimal configuration of the system under the input constraints. Then, the solved configuration is returned to the WDM VLC system model to evaluate the system's energy efficiency (EE^{TL}).
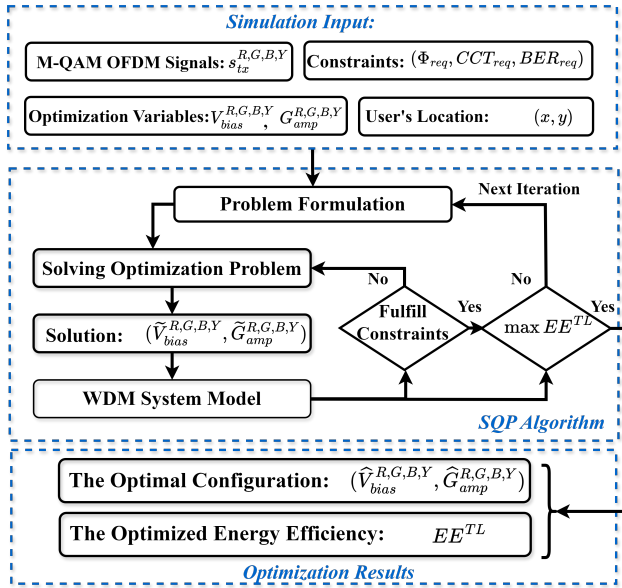

Fig. 8: Schematic diagram of the simulation process

Fig. 8 details the process of the simulation. The variables are generated and bounded following the values in Tab. II. The user's location is initiated as a uniform distribution within the $2m \times 2m$ broadcasting coverage at a $20cm$ step width. The user's requirements of illuminance (Φ_{req}), illumination color (CCT_{req}), and threshold BER of each channel (BER_{req}) are quantified into constraints. These quantities form the simulation input.

Consequently, the formulated optimization problem is solved by the SQP algorithm. During each iteration, the solved configuration ($\widetilde{V}_{bias}^{R,G,B,Y}, \widetilde{G}_{amp}^{R,G,B,Y}$) is assessed through the WDM VLC system model to confirm its adherence to the constraints. Iterations continue until a configuration maximizing the system's energy efficiency is identified, at which point the optimal configuration($\widehat{V}_{bias}^{R,G,B,Y}, \widehat{G}_{amp}^{R,G,B,Y}$), and optimized energy efficiency (EE^{TL}) are returned.

2) Optimization Performance: To validate the performance of the proposed method, each point of the simulated area is traversed to implement a whole process of the optimization and compare the results with the control group, labeled "Optimized" and "Unoptimized" in the legend. The control group behaves as a conventional optimization, in which the system maintains a fixed configuration with minimal power consumption under the constraints. The constraints for illuminance and CCT are constantly set as $\Phi_{Rx}^{req} \geq 200lx$, and $CCT \leq 5000K$, satisfying the indoor illumination standards for an office environment [35]. The BER is required lower than $BER^{R,G,B,Y} \leq 10^{-5}$ for each channel, respecting the wireless communication requirement [31]. Fig. 9 displays the optimization results of system transmitting 16-QAM and 32-QAM OFDM signals.

In the Fig. 9 (a), the proposed optimization method achieves the highest energy efficiency of 6.25×10^7 (bit/J) at the location (0,0), whereas the control group reaches 2.37×10^7 (bit/J). At the boundary, both methods yield an energy efficiency of 1.63×10^7 (bit/J). The average values of each user's location for the proposed method and control group are 4.13×10^7 (bit/J) and 2.05×10^7 (bit/J), respectively. In 32-QAM transmission, shown in Fig. 9 (b), the proposed method and the control group achieve peak energy efficiencies of 5.46×10^7 (bit/J) and 1.74×10^7 (bit/J) with the average values of each location 3.44×10^7 (bit/J) and 1.51×10^7 (bit/J), respectively.

The proposed method calculates the most cost-effective signal power subject to the given constraints, thereby yielding double energy efficiency compared to the conventional approach. Furthermore, the average energy efficiency enhancement of the proposed method increases from 101% to 127% with the modulation format from 16-QAM to 32-QAM. Because, under equivalent conditions, a higher data rate demands increased energy consumption, whereas the optimization effect becomes more pronounced.

3) Generality Validation: As the performance of the proposed optimization method is evaluated under a fixed constraints condition, its generality applying to different communication and illumination requirements are validated in this section. Initially, it is assumed that the broadcasting system serves for diverse users, where differentiation between user data is achieved through frequency division multiplexing. Consequently, the proposed optimization method must be adaptable to scenarios wherein the system transmits signals across varying central frequencies. Subsequently, in consideration of
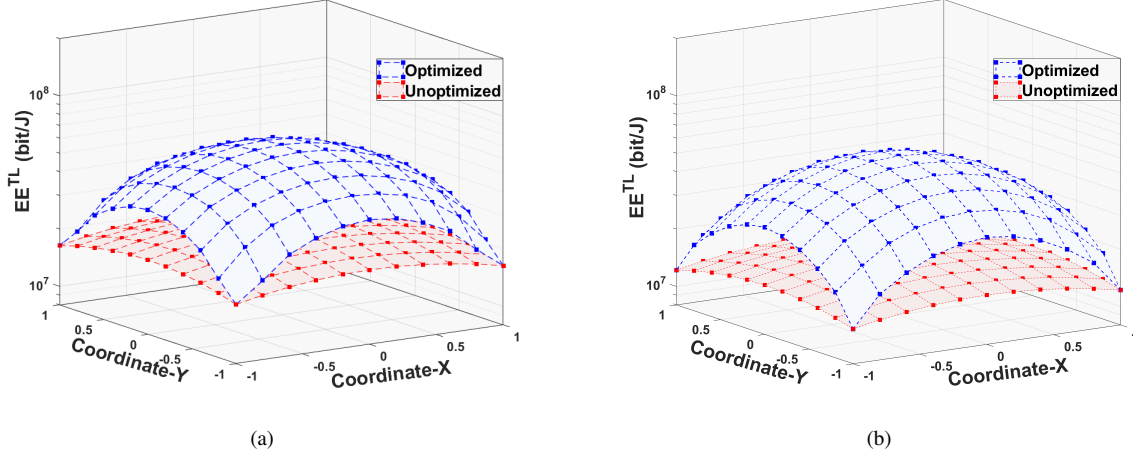
(a)

(b)

Fig. 9: Optimized energy efficiency when the user is at different locations: (a) Transmitted 16-QAM-OFDM signal, and (b) Transmitted 32-QAM-OFDM signal.

the varied illumination demands of users, the proposed method is required to be applicable to scenarios wherein the system provides diverse intensities and visual colors of illumination.

Case(1) Different signal frequencies. : The user is fixed at the coordinate $(0,0)$, and the illumination constraints are set at $\Phi_{Rx}^{req} \geq 400lx$, and $CCT \leq 5000K$, simulating the illumination requirements of an indoor reading scenario. The BER is set as $BER^{R,G,B,Y} \leq 10^{-5}$. OFDM signals for 16-QAM, 32-QAM, and 64-QAM, with central frequencies ranging from 5MHz to 30MHz, are used in the broadcast service. Fig. 10 illustrates optimized energy efficiency (EE^{TL}) and corresponding communication power consumption for each central frequency.
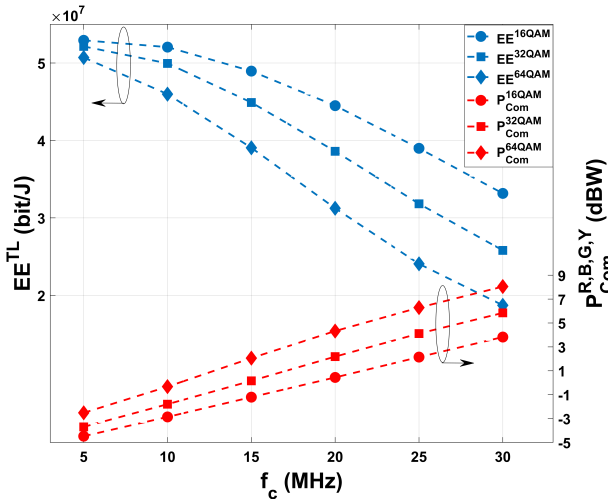

Fig. 10: Optimized energy efficiency at different signal's central frequency.

Applying the proposed method, optimized energy efficiency EE^{TL} decreases sequentially from 5×10^7 (bit/J) to 3.32×10^7 (bit/J), 2.58×10^7 (bit/J), and 1.87×10^7(bit/J) for 16-QAM, 32-QAM, and 64-QAM OFDM signal transmission, respec-

tively. Concurrently, the signal power consumption across four channels escalates from -4.47 dBW, -3.69 dBW, and -2.52 dBW to 3.82 dBW, 5.84 dBW, 8.04 dBW, respectively.

Two key insights are gleaned from these results. First, they confirm the practical understanding that higher data rates necessitate greater signal power. Second, the results align with the measured response of the WDM VLC system, indicating that signal power loss significantly rises with increasing signal frequency. The system's generality across varied transmitted signal frequencies is attributable to the accurate LED model.

Case(2) Diverse illumination requirements: To further evaluate the generality of the proposed method on diverse illumination requirements. the user is fixed on the location $(0,0)$, and the BER is required as $BER^{R,G,B,Y} \leq 10^{-5}$. The constraints of user-required illuminance (Φ^{req}) and illumination color (CCT^{req}) vary from $300lx$ to $600lx$ and $3000K$ to $5000K$, respectively, almost covering the indoor illumination scenarios following the CIE standards [35]. Fig. 11 (a) and (b) depict the optimized energy efficiency in response to these different illumination requirements, along with the corresponding communication power consumption ($P_{com}^{R,G,B,Y}$).

In Fig. 11 (a), energy efficiency markedly declines as required illuminance increases. It is noteworthy that the power consumption for communication increases with the required illuminance. This phenomenon is consistent with the measurements shown in Fig. 6 that signal power loss increases with the applied voltage. The system requires more signal power to maintain the response while providing higher illuminance. The mechanism behind this phenomenon lies in the interplay between the illumination and communication functionalities of the LED.

In Fig. 11 (b), higher CCT values, corresponding to cooler white light, result in improved energy efficiency. It is because higher CCT values permit more blue components contained in the output light of the RGBY-LED. Due to the superior electroluminescence characteristics of the blue sub-LED in the
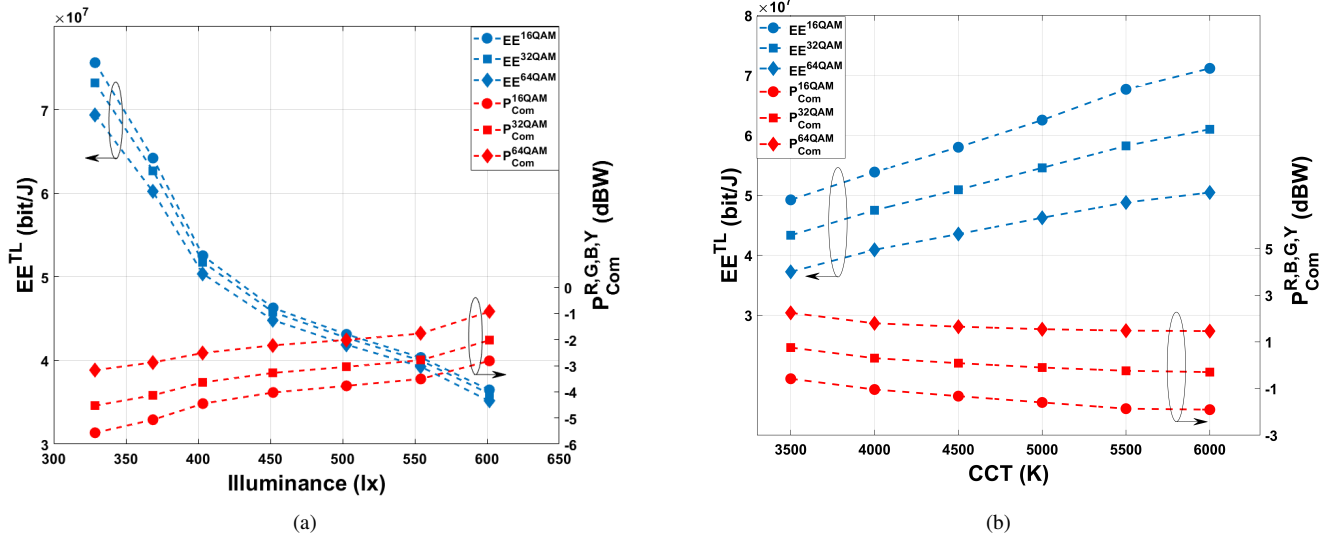
Fig. 11: (a) Optimized energy efficiency at different user-required illuminance (b) The optimized energy efficiency at different user-required illumination colors.

RGBY-LED system, as demonstrated in Fig. 4, when the blue sub-LED predominates in the illumination service, other sub-LEDs require less power, reducing overall illumination power consumption and thereby enhancing system energy efficiency. Meanwhile, it is evident that the communication power consumption is also reduced, which further increases the system's energy efficiency. Because, the reduction of the illumination power consumption requiring lower bias voltages ($V_{bias}^{R,G,Y}$) of the RGBY-LED, resulting in the higher signal response of the system, as Fig. 6 proved. Thus, less signal power is consumed during the data transmission. This phenomenon also comes from the interplay between the illumination and communication performance of the system.

In these simulations, the optimization results of the proposed method accordingly vary with the illumination requirements, and the tendency of the variations is consistent with the physical mechanism and the experimental measurements. Therefore, the proposed method can be generalized to optimize the energy efficiency of the WDM VLC system under different scenarios.

V. CONCLUSION

In this paper, a novel optimization method is proposed for RGBY-LED based WDM VLC systems. A physics-based LED model is integrated with the transmission channel, and WDM receiver models, forming the system model. It characterizes the signal response and illumination performance across different color channels and quantifies the interplay of them. The energy efficiency of the WDM VLC system is defined and formulated into an optimization problem with the constraints following the indoor illumination standard and communication quality. The proposed optimization method, validated on the experimental-based simulation, achieves the double performance of the conventional. Moreover, it exhibits a strong generality to adapt to diverse scenarios, highlighting its potential for practical implementations.

In traditional communication systems, maximizing data rates and minimizing power consumption are primary objectives. However, VLC brings an additional layer of complexity with the need to meet illumination requirements. The proposed energy efficiency optimization method successfully addresses this critical challenge, demonstrating that the optimal energy efficiency of a VLC system is not merely tied to minimizing power consumption. Instead, it's about striking a balance between communication and illumination demands.

APENDIX-I

The parameter functions in the section II-A which describes the internal physics of the LED are derived as Eq. (38) to (51). The definition of the parameters are listed in TAB III. For convenient illustration in section III-C, the constraint equations are unexpanded, the original expressions are shown as Eq. (52) to (55).

$$z_n(V_j) = \frac{r_{qn}}{n \cdot (r_n + r_b) + r_{qn}} \tag{38}$$

$$n^* = \frac{m^* k_B T}{\pi \hbar^2 L_q} \tag{39}$$

$$a_1(V_j) = \eta_{ph} \beta_{sp} n R_{ph} z_n(V_j) \tag{40}$$

$$a_2 = R_{ph} C_{ph} \tag{41}$$

$$a_3(V_j) = (r_q + n \cdot z_n) \cdot (Z_s + R_s) + r_q z_n \tag{42}$$

$$a_4(V_j) = r_q z_n C_e (Z_s + R_s) \tag{43}$$

$$a_5(V_j) = n\eta_{ph}R_{ph}\beta_{sp}qA_qL_q\gamma_2(n^*)^2$$
$$\cdot \ln\left[1 + \exp\left(\frac{\alpha_1 V_j + \alpha_2 V_j^2 + \alpha_3 V_j^3}{k_B T}\right)\right]^2 \quad (44)$$

TABLE III: Definition of Terms.

Terminology	Definition
$A_{c,q,b}$	Transection area of each layer
A_{eff}	Effective area of barrier
A_{rec}	Area of photo-receiver
$\alpha_{1,2,3}$	Coefficient of the fitting curve
β_{sp}	Spontaneous emission coefficient
C	Capacitance
D	Distance between LED and VLC receiver
γ_1	Coefficient of the SRH recombination
γ_2	Coefficient of the radiative recombination
γ_3	Coefficient of the Auger recombination
$\epsilon_{q,b}$	Relative dielectric constant of the layer
$\Phi_{\frac{1}{2}}$	Semi-angle at half-power of LED
$\hbar$	Reduced Planck constant
$I_{c,q,b}$	Current of each layer
I_j	Injected current of LED
I_s	Reverse bias saturation current
k_B	Boltzmann constant
κ	Sensitivity of APD
L	Thickness of the layer
n	number of the quantum wells
μ	Order of Lambertian radiation
N_D^+	Ionized donors density
N_A^+	Ionized acceptors density
η	Ideal factor of diode
η_L	Efficacy of LED
η_{ph}	Light extraction rate
P	Power
q	Elementary charge
θ	Angle of receiving direction in VLC channel
R	Constant resistance
r	Differential resistance
$\sigma_{th,short}$	Thermal and short noise power
T	Temperature
τ_b	Effective space transport time
τ_{ph}	Photons lifetime
V_D	Potential difference of the barrier
V_j	Junction voltage
ψ	Angle of transmission direction in VLC channel
Z	Impedance

REFERENCES

[1] M. Boldi *et al.*, "6g architecture landscape–european perspective," *5G Architecture Working Group, 5G PPP, Tech. Rep*, 2022.

[2] D. C. Nguyen, M. Ding, P. N. Pathirana, A. Seneviratne, J. Li, D. Niyato, O. Dobre, and H. V. Poor, "6g internet of things: A comprehensive survey," *IEEE Internet of Things Journal*, vol. 9, no. 1, pp. 359–383, 2021.

[3] M. Shehab, T. Khattab, M. Kucukvar, and D. Trinchero, "The role of 5g/6g networks in building sustainable and energy-efficient smart cities," in *2022 IEEE 7th International Energy Conference (ENERGYCON)*. IEEE, 2022, pp. 1–7.

[4] A. Mourad, R. Yang, P. H. Lehne, and A. De La Oliva, "Towards 6g: Evolution of key performance indicators and technology trends," in *2020 2nd 6G wireless summit (6G SUMMIT)*. IEEE, 2020, pp. 1–5.

[5] M. Z. Chowdhury, M. Shahjalal, S. Ahmed, and Y. M. Jang, "6g wireless communication systems: Applications, requirements, technologies, challenges, and research directions," *IEEE Open Journal of the Communications Society*, vol. 1, pp. 957–975, 2020.

[6] L. E. M. Matheus, A. B. Vieira, L. F. Vieira, M. A. Vieira, and O. Gnawali, "Visible light communication: concepts, applications and challenges," *IEEE Communications Surveys & Tutorials*, vol. 21, no. 4, pp. 3204–3237, 2019.

[7] N. Chi, Y. Zhou, Y. Wei, and F. Hu, "Visible light communication in 6g: Advances, challenges, and prospects," *IEEE Vehicular Technology Magazine*, vol. 15, no. 4, pp. 93–102, 2020.

[8] S. Ariyanti and M. Suryanegara, "Visible light communication (vlc) for 6g technology: The potency and research challenges," in *2020 Fourth world conference on smart trends in systems, security and sustainability (WorldS4)*. IEEE, 2020, pp. 490–493.

[9] J. Shi, W. Niu, Y. Ha, Z. Xu, Z. Li, S. Yu, and N. Chi, "Ai-enabled intelligent visible light communications: Challenges, progress, and future," in *Photonics*, vol. 9, no. 8. MDPI, 2022, p. 529.

[10] M. Kashef, M. Ismail, M. Abdallah, K. A. Qaraqe, and E. Serpedin, "Energy efficient resource allocation for mixed rf/vlc heterogeneous wireless networks," *IEEE Journal on Selected Areas in Communications*, vol. 34, no. 4, pp. 883–893, 2016.

[11] A. Khreishah, S. Shao, A. Gharaibeh, M. Ayyash, H. Elgala, and N. Ansari, "A hybrid rf-vlc system for energy efficient wireless access," *IEEE Transactions on Green Communications and Networking*, vol. 2, no. 4, pp. 932–944, 2018.

[12] S. Aboagye, A. Ibrahim, T. M. Ngatched, A. R. Ndjiongue, and O. A. Dobre, "Design of energy efficient hybrid vlc/rf/plc communication system for indoor networks," *IEEE Wireless Communications Letters*, vol. 9, no. 2, pp. 143–147, 2019.

[13] L. Li, Y. Zhang, B. Fan, and H. Tian, "Mobility-aware load balancing scheme in hybrid vlc-lte networks," *IEEE Communications Letters*, vol. 20, no. 11, pp. 2276–2279,

$$r_n(V_j) = \frac{\eta k_B T}{n_0 q^2 A_c L_c \exp\left(\frac{qV_j}{\eta k_B T}\right)(\gamma_1 + 3\gamma_3 \cdot n_0^2 \exp^2\left(\frac{qV_j}{\eta k_B T}\right))} \tag{45}$$

$$r_b(V_j) = \frac{\tau_b}{q \cdot n^* A_b L_b} \left[\frac{\exp\left(\frac{\alpha_1 Vj + \alpha_2 V_j^2 + \alpha_3 V_j^3}{k_B T}\right) \cdot (\alpha_1 + 2\alpha_2 V_j + 3\alpha_3 V_j^2)}{k_B T[1 + \exp\left(\frac{\alpha_1 V_j + \alpha_2 V_j^2 + \alpha_3 V_j^3}{k_B T}\right)]} \cdot \exp\left(\frac{q(V_j - V_D)}{k_B T}\right) \right. \tag{46}$$

$$\left. + \frac{q}{k_B T} \cdot \ln[1 + \exp\left(\frac{\alpha_1 V_j + \alpha_2 V_j^2 + \alpha_3 V_j^3}{k_B T}\right)] \cdot \exp\left(\frac{q(V_j - V_D)}{k_B T}\right) \right]^{-1} \tag{47}$$

$$r_{qn}(V_j) = \frac{k_B T[1 + \exp\left(\frac{\alpha_1 V_j + \alpha_2 V_j^2 + \alpha_3 V_j^3}{k_B T}\right)]}{qn^* A_q L_q \exp\left(\frac{\alpha_1 V_j + \alpha_2 V_j^2 + \alpha_3 V_j^3}{k_B T}\right)(\alpha_1 + 2\alpha_2 V_j^2 + 3\alpha_3 V_j^2)} \cdot \frac{1}{\gamma_1 + 3\gamma_3[n^* \ln(1 + \exp\left(\frac{\alpha_1 V_j + \alpha_2 V_j^2 + \alpha_3 V_j^3}{k_B T}\right))]^2} \tag{48}$$

$$r_{qr}(V_j) = \frac{k_B T[1 + \exp\left(\frac{\alpha_1 V_j + \alpha_2 V_j^2 + \alpha_3 V_j^3}{k_B T}\right)]}{2(n^*)^2 qn^* A_q L_q \exp\left(\frac{\alpha_1 V_j + \alpha_2 V_j^2 + \alpha_3 V_j^3}{k_B T}\right)(\alpha_1 + 2\alpha_2 V_j^2 + 3\alpha_3 V_j^2)} \cdot \frac{1}{\ln(1 + \exp\left(\frac{\alpha_1 V_j + \alpha_2 V_j^2 + \alpha_3 V_j^3}{k_B T}\right))} \tag{49}$$

$$C_e(V_j) = \frac{q^2 n_0 A_c L_c}{\eta k_B T} \exp\left(\frac{qV_j}{\eta k_B T}\right) + n \cdot \frac{q A_q L_q n^* \exp\left(\frac{\alpha_1 V_j + \alpha_2 V_j^2 + \alpha_3 V_j^3}{k_B T}\right)}{k_B T(1 + \exp\left(\frac{\alpha_1 V_j + \alpha_2 V_j^2 + \alpha_3 V_j^3}{k_B T}\right))} \tag{50}$$

$$\cdot (\alpha_1 + 2\alpha_2 V_j + 3\alpha_3 V_j^2) + A_{eff}\left[\frac{q\epsilon_q \epsilon_b N_A N_D}{2(\epsilon_q N_D + \epsilon_b N_A)} \frac{1}{V_D - V_j}\right]^{\frac{1}{2}} \tag{51}$$

$$\Phi_{Rx}(\boldsymbol{V_{bias}}) = 638 \cdot \eta_{ph} R_{ph} \cdot n\beta_{sp} q A_q L_q \gamma_2 \cdot \frac{(\mu+1) \cdot cos(\psi)^\mu cos(\theta)}{2\pi D^2} \cdot \int_{380}^{830} \mathcal{V}(\lambda) \exp\left(\frac{-4(\lambda - \lambda_0)^2}{(\Delta\lambda)^2}\right) d\lambda$$

$$\cdot \left[n^* \ln\left(1 + \exp\left(\frac{\alpha_1 \boldsymbol{V_{bias}} - I_{DC} R_s + \alpha_2(\boldsymbol{V_{bias}} - I_{DC} R_s)^2 + \alpha_3(\boldsymbol{V_{bias}} - I_{DC} R_s)^3}{k_B T}\right)\right)\right]^2 \tag{52}$$

$$BER(\boldsymbol{V_{bias}}, \boldsymbol{G_{amp}}) = \frac{4}{\log_2(M)}(1 - \frac{1}{\sqrt{M}})Q\left(\sqrt{\frac{3\log_2(M)}{M-1}\mathsf{SNR}}\right) = \frac{4}{\log_2(M)}(1 - \frac{1}{\sqrt{M}})Q\left\{\sqrt{\frac{3\log_2(M)}{(M-1)(\sigma_{th}^2 + \sigma_{shot}^2)}}\right.$$

$$\cdot \frac{\boldsymbol{G_{amp}} \cdot G_{opt} \cdot a_1(\boldsymbol{V_{bias}} - I_{DC} R_s)}{a_4(\boldsymbol{V_{bias}} - I_{DC} R_s) - a_2 \cdot a_3(\boldsymbol{V_{bias}} - I_{DC} R_s)} \cdot \frac{(\mu+1)A_{rec} \cdot cos(\psi)^\mu cos(\theta)}{2\pi D^2} \cdot \int_{\lambda_{min}}^{\lambda_{max}} \Gamma_p \text{rect}(\frac{\lambda - \lambda_c}{\Delta\lambda}) \cdot$$

$$\exp\left(\frac{-4(\lambda - \lambda_0)^2}{(\Delta\lambda)^2}\right) \cdot \kappa(\lambda) d\lambda \cdot \int_{-\infty}^{+\infty} \left[\exp\left(\frac{-a_3(\boldsymbol{V_{bias}} - I_{DC} R_s) \cdot t}{a_4(\boldsymbol{V_{bias}} - I_{DC} R_s)}\right) - \exp\left(\frac{-t}{a_2}\right)\right] \cdot s_{tx}(t - \tau) d\tau \right\} \tag{53}$$

$$CCT(\boldsymbol{V_{bias}^{R,G,B,Y}}) = 437 \cdot \hat{n}^3(\boldsymbol{V_{bias}^{R,G,B,Y}}) + 3601 \cdot \hat{n}^2(\boldsymbol{V_{bias}^{R,G,B,Y}}) + 6861 \cdot \hat{n}(\boldsymbol{V_{bias}^{R,G,B,Y}}) + 5517 \tag{54}$$

$$\hat{n}(\boldsymbol{V}_{bias}^{\boldsymbol{R,G,B,Y}}) = \frac{\int_{380}^{830} \bar{x}(\lambda) P_L^{TL}(\lambda, \boldsymbol{V}_{bias}^{\boldsymbol{R,G,B,Y}}) d\lambda}{\int_{380}^{830} P_L^{TL}(\lambda, \boldsymbol{V}_{bias}^{\boldsymbol{R,G,B,Y}})(\bar{x}(\lambda) + \bar{y}(\lambda) + \bar{z}(\lambda)) d\lambda} - 0.3320$$

$$\cdot \left(0.1858 - \frac{\int_{380}^{830} \bar{y}(\lambda) P_L^{TL}(\lambda, \boldsymbol{V}_{bias}^{\boldsymbol{R,G,B,Y}}) d\lambda}{\int_{380}^{830} P_L^{TL}(\lambda, \boldsymbol{V}_{bias}^{\boldsymbol{R,G,B,Y}})(\bar{x}(\lambda) + \bar{y}(\lambda) + \bar{z}(\lambda)) d\lambda} \right)^{-1} \tag{55}$$

2016.

[14] A. Al Hammadi, S. Muhaidat, P. C. Sofotasios, and M. Al Qutayri, "A robust and energy efficient noma-enabled hybrid vlc/rf wireless network," in *2019 IEEE Wireless Communications and Networking Conference (WCNC)*. IEEE, 2019, pp. 1–6.

[15] S. Aboagye, A. Ibrahim, T. M. Ngatched, and O. A. Dobre, "Vlc in future heterogeneous networks: Energy– and spectral–efficiency optimization," in *ICC 2020-2020 IEEE International Conference on Communications (ICC)*. IEEE, 2020, pp. 1–7.

[16] M. Obeed, A. M. Salhab, M.-S. Alouini, and S. A. Zummo, "On optimizing vlc networks for downlink multi-user transmission: A survey," *IEEE Communications Surveys & Tutorials*, vol. 21, no. 3, pp. 2947–2976, 2019.

[17] L. An, H. Shen, J. Wang, Y. Zeng, and R. Ran, "Energy efficiency optimization for mimo visible light communication systems," *IEEE Wireless Communications Letters*, vol. 9, no. 4, pp. 452–456, 2019.

[18] S. I. Mushfique, A. Alsharoa, and M. Yuksel, "Optimization of sinr and illumination uniformity in multi-led multi-datastream vlc networks," *IEEE Transactions on Cognitive Communications and Networking*, vol. 6, no. 3, pp. 1108–1121, 2020.

[19] Z. Cheng, X. Wang, L. Xia, Y. Yuan, J. Jin, and Q. Wang, "Correlation based lamp selection scheme under illumination constraint for vlc mimo systems," in *2021 International Wireless Communications and Mobile Computing (IWCMC)*. IEEE, 2021, pp. 2103–2108.

[20] S. Ma, T. Zhang, S. Lu, H. Li, Z. Wu, and S. Li, "Energy efficiency of siso and miso in visible light communication systems," *Journal of Lightwave Technology*, vol. 36, no. 12, pp. 2499–2509, 2018.

[21] X. Deng, W. Fan, T. E. B. Cunha, S. Ma, C. Chen, Y. Dong, X. Zou, L. Yan, and J.-P. M. Linnartz, "Two-dimensional power allocation for optical mimo-ofdm systems over low-pass channels," *IEEE Transactions on Vehicular Technology*, vol. 71, no. 7, pp. 7244–7257, 2022.

[22] S. Chatterjee and D. Sabui, "Daylight integrated indoor vlc architecture: an energy-efficient solution," *Transactions on Emerging Telecommunications Technologies*, vol. 31, no. 9, p. e3800, 2020.

[23] T. Tang, T. Shang, Q. Li, G. Li, and B. Bai, "Energy-efficient subchannel assignment and power allocation in vlc-iot systems with slipt," *Optics Express*, vol. 30, no. 22, pp. 39 492–39 509, 2022.

[24] X. Deng, W. Fan, T. E. B. Cunha, S. Ma, C. Chen, Y. Dong, X. Zou, L. Yan, and J.-P. M. Linnartz, "Two-dimensional power allocation for optical mimo-ofdm systems over low-pass channels," *IEEE Transactions on Vehicular Technology*, vol. 71, no. 7, pp. 7244–7257, 2022.

[25] P. Salvador, J. Valls, M. J. Canet, V. Almenar, and J. L. Corral, "On the performance and power consumption of bias-t based drivers for high speed vlc," *Journal of Lightwave Technology*, vol. 40, no. 18, pp. 6078–6086, 2022.

[26] S. Ma, T. Zhang, S. Lu, H. Li, Z. Wu, and S. Li, "Energy efficiency of siso and miso in visible light communication systems," *Journal of Lightwave Technology*, vol. 36, no. 12, pp. 2499–2509, 2018.

[27] J. Gancarz, H. Elgala, and T. D. Little, "Impact of lighting requirements on vlc systems," *IEEE Communications Magazine*, vol. 51, no. 12, pp. 34–41, 2013.

[28] D. Shi, J. Li, Y. Liu, L. Shi, Y. Huang, Z. Wang, X. Zhang, and A. Vladimirescu, "Effect of illumination intensity on led based visible light communication system," in *2020 IEEE International Symposium on Broadband Multimedia Systems and Broadcasting (BMSB)*. IEEE, 2020, pp. 1–4.

[29] X. Deng, Y. Wu, A. Khalid, X. Long, and J.-P. M. Linnartz, "Led power consumption in joint illumination and communication system," *Optics express*, vol. 25, no. 16, pp. 18 990–19 003, 2017.

[30] T. Smith and J. Guild, "The cie colorimetric standards and their use," *Transactions of the optical society*, vol. 33, no. 3, p. 73, 1931.

[31] R. Bian, I. Tavakkolnia, and H. Haas, "15.73 gb/s visible light communication with off-the-shelf leds," *Journal of Lightwave Technology*, vol. 37, no. 10, pp. 2418–2424, 2019.

[32] Y. Wang, L. Tao, X. Huang, J. Shi, and N. Chi, "8-gb/s rgby led-based wdm vlc system employing high-order cap modulation and hybrid post equalizer," *IEEE photonics journal*, vol. 7, no. 6, pp. 1–7, 2015.

[33] F. Wu, C.-T. Lin, C. Wei, C. Chen, Z. Chen, H. Huang, and S. Chi, "Performance comparison of ofdm signal and cap signal over high capacity rgb-led-based wdm visible light communication," *IEEE photonics journal*, vol. 5, no. 4, pp. 7 901 507–7 901 507, 2013.

[34] D. Shi, X. Zhang, Z. Liu, X. Chen, X. Liu, J. Wang, J. Song, and A. Vladimirescu, "Physics-based modeling of gan mqw led for visible light communication systems," *IEEE Transactions on Electron Devices*, 2023.

[35] J. Schanda, *Colorimetry: understanding the CIE system*. John Wiley & Sons, 2007.

[36] J. Azaña and M. A. Muriel, "Real-time optical spectrum analysis based on the time-space duality in chirped fiber gratings," *IEEE Journal of quantum electronics*, vol. 36, no. 5, pp. 517–526, 2000.

[37] C. S. McCamy, "Correlated color temperature as an explicit function of chromaticity coordinates," *Color Research & Application*, vol. 17, no. 2, pp. 142–144, 1992.

[38] Y. Qiu, H.-H. Chen, and W.-X. Meng, "Channel modeling for visible light communications—a survey," *Wireless Communications and Mobile Computing*, vol. 16, no. 14, pp. 2016–2034, 2016.

[39] K. M. Johnson, "High-speed photodiode signal enhancement at avalanche breakdown voltage," *IEEE Transactions on Electron Devices*, vol. 12, no. 2, pp. 55–63, 1965.

[40] W. Haemers *et al.*, "An upper bound for the shannon capacity of a graph," in *Colloq. Math. Soc. János Bolyai*, vol. 25. Hungary, 1978, pp. 267–272.

[41] G. Tosini, I. Ferguson, and K. Tsubota, "Effects of blue light on the circadian system and eye physiology," *Molecular vision*, vol. 22, p. 61, 2016.

[42] A. D. Ellis, J. Zhao, and D. Cotter, "Approaching the non-linear shannon limit," *Journal of lightwave technology*, vol. 28, no. 4, pp. 423–433, 2009.

[43] G. K. Karagiannidis and A. S. Lioumpas, "An improved approximation for the gaussian q-function," *IEEE Communications Letters*, vol. 11, no. 8, pp. 644–646, 2007.

[44] P. E. Gill, W. Murray, and M. A. Saunders, "Snopt: An sqp algorithm for large-scale constrained optimization," *SIAM review*, vol. 47, no. 1, pp. 99–131, 2005.

[45] D. C. Liu and J. Nocedal, "On the limited memory bfgs method for large scale optimization," *Mathematical programming*, vol. 45, no. 1-3, pp. 503–528, 1989.

[46] F. Hu, G. Li, P. Zou, J. Hu, S. Chen, Q. Liu, J. Zhang, F. Jiang, S. Wang, and N. Chi, "20.09-gbit/s underwater wdm-vlc transmission based on a single si/gaas-substrate multichromatic led array chip," in *2020 Optical fiber communications conference and exhibition (OFC)*. IEEE, 2020, pp. 1–3.

[47] S. Lee, J. Kwon, S. Jung, and Y. Kwon, "Simulation modeling of visible light communication channel for automotive applications," in *2012 15th International IEEE Conference on Intelligent Transportation Systems*. IEEE, 2012, pp. 463–468.